

Alignment and characterization of high uniformity imaging spectrometers

Holly A. Bender*, Pantazis Mouroulis, Michael L. Eastwood, Robert O. Green,
Sven Geier, Eric B. Hochberg
Jet Propulsion Laboratory, California Institute of Technology

ABSTRACT

Imaging spectrometers require precise adjustments, in some cases at the sub-micrometer level, in order to achieve a uniform response over both the spectral and spatial dimensions. We describe a set of measurement techniques and their corresponding alignment adjustments to achieve the 95% or higher uniformity specifications required for Earth-observing imaging spectrometers. The methods are illustrated with measurements from the Next Generation Imaging Spectrometer system that has been built at the Jet Propulsion Laboratory, California Institute of Technology, under contract with the National Aeronautics and Space Administration.

Keywords: imaging spectroscopy, Offner spectrometer, optical alignment

1. INTRODUCTION

Pushbroom imaging spectrometers offer advantages in remote sensing due to their high resolution capabilities and high signal-to-noise data products. However, in order to extract the accurate spectral signatures needed for remote sensing applications, the instrument must maintain a high level of uniformity and undergo an accurate characterization and calibration process.

The uniformity requirement may be summarized as follows. In the spectral domain, it is required that the instrument spectral response function (SRF) be independent of field position. In the spatial domain, it is required that the spatial response function be independent of wavelength. In the latter case, we distinguish between cross-track spatial response function (CRF) and along-track spatial response function (ARF). The requirement for wavelength invariance applies to both. The variation of SRF with wavelength or of CRF/ARF with field is not part of the uniformity problem as it does not lead to artifacts in the recovered data.

However desirable it may be, it is impractical to demand complete invariance of the response functions. The uniformity problem is thus simplified using the first and second moments of those functions. To the extent that they can be reasonably well described by Gaussians or other similar forms, we therefore demand that the following five parameters be invariant:

- 1) The SRF centroid coordinate in the spatial direction (no “smile”)
- 2) The SRF width (half-width (FWHM) or standard deviation)
- 3) The CRF centroid coordinate in the spectral direction (no “keystone”)
- 4) The CRF width (half-width or standard deviation)
- 5) The ARF width (half-width or standard deviation)

Subtle variations in the response function shape may remain even after the above conditions are satisfied in systems where the response functions are not sufficiently well characterized by symmetric functions like a Gaussian or a Lorentzian. However, these additional variations are outside the scope of this paper.

Corresponding author: *holly.a.bender@jpl.nasa.gov; Phone: 1 818 393-6424; Fax: 1 818 393-3290; Address: Jet Propulsion Laboratory, 4800 Oak Grove Drive, MS 306-392, Pasadena, CA 91109.

Specifically, it has been shown that spectral and spatial non-uniformity values must be kept within a small fraction of a pixel in order to meet the standards of high performance imaging spectroscopy¹⁻². Typical desired values for geometric uniformity are <5% of a pixel (or <1.3 μm for our 27 μm detector pixel), and <10% for FWHM variation². Research has been done in various post-processing techniques for smile correction³ or keystone correction⁴ through re-sampling. However, re-sampling techniques are not always possible to employ, and in any case minimizing these errors from the start is key to avoiding an unnecessarily complex data reduction process.

This paper will discuss how such high uniformity may be successfully achieved in practice through the alignment and characterization of several imaging spectrometers developed at NASA's Jet Propulsion Laboratory (JPL) under the Next-Generation airborne Imaging Spectrometer (NGIS) project. The manner in which such uniformity has been achieved at the design level and through detailed tolerancing has been previously discussed⁵.

2. OPTICAL DESIGN AND WARM ALIGNMENT

2.1 Design overview

The NGIS design⁵ consists of a two-mirror anastigmat telescope and an Offner-type spectrometer⁶⁻⁷. The primary and tertiary spectrometer surfaces are concave and concentric silver-coated glass mirrors, while the secondary is a coaxial triple-blazed convex grating designed and fabricated at JPL. Operating in first order, the grating is split into three concentric zones with differing blaze angles tailored to meet a specific response function. A lithographically-fabricated slit measuring 27 μm wide and 16.2 mm long is located in front of the spectrometer optics and itself is preceded by the two-mirror telescope. A single focal plane array covers the entire solar reflected spectrum from 380 to 2510nm and is coupled with a specially designed order sorting filter. A schematic of the NGIS design is shown in Fig. 1.

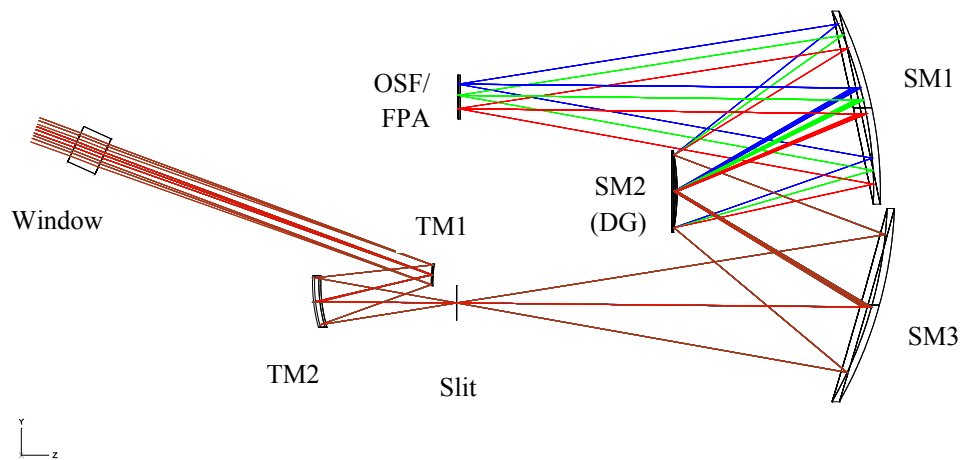


Figure 1: NGIS optical design (TM1 and TM2 are the primary and secondary telescope mirrors, SM1 and SM3 are the primary and tertiary spectrometer mirrors, SM2 (DG) is the diffraction grating, OSF is an order sorting filter, FPA is the focal plane array detector, and Window is the instrument vacuum window.)

2.2 Instrument warm alignment

The telescope, working at F/3 with a 33.5 degree field of view, consists of two aluminum-coated aspheres. Due to the minimalist nature of the design, only a simple snap-together assembly and alignment was required to meet the wavefront error requirement of <1.44 waves peak-to-valley and <0.227 waves rms. A final interferogram of one of the NGIS telescope units is shown in Fig. 2.

A typical spectrometer alignment process is detailed in Ref. 8, but requires some modifications in our case due to the grating apodization. The spectrometer operates in first order, but the diagnostic aberration is largely observed in third order. Using an interferometer and a spherical return mirror we take interferograms in both 1st and 3rd order through field. The measured interferometric error (deviation from desired) is modeled in Zemax in order to derive the misalignment condition. This is done iteratively for the two orders and three field positions. Fig. 3 shows the close interferometric match we are able to achieve to the design. While only third order is shown here, it should be noted that first order interferograms are used in the process as well.

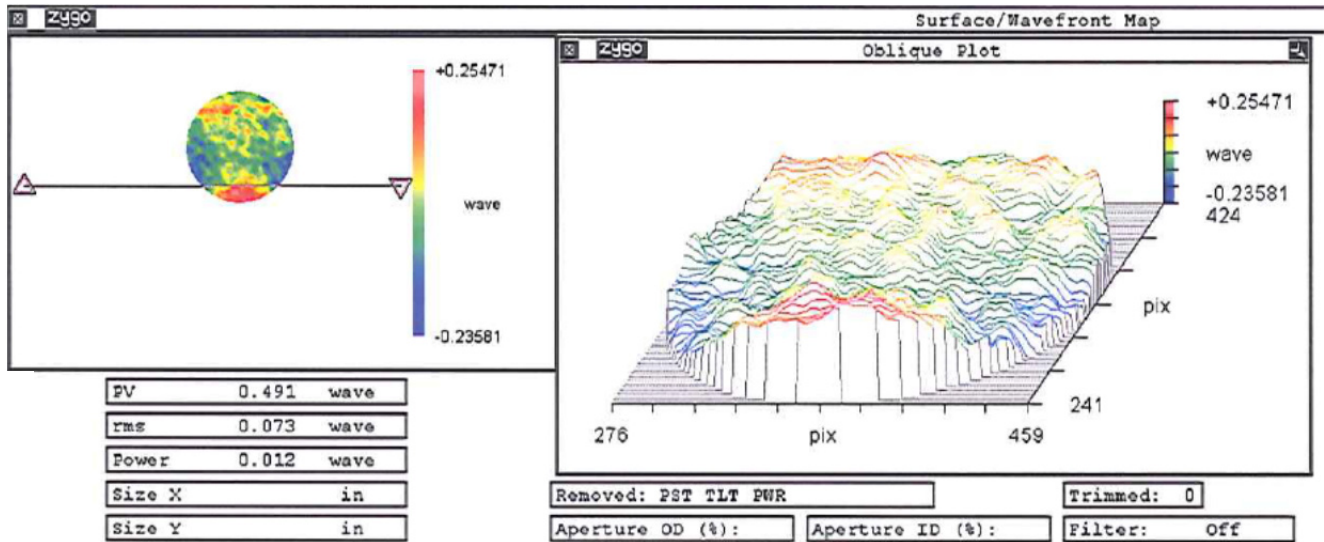


Figure 2: An NGIS telescope interferogram demonstrates wavefront error of 0.49 waves P-V and 0.073 waves rms.

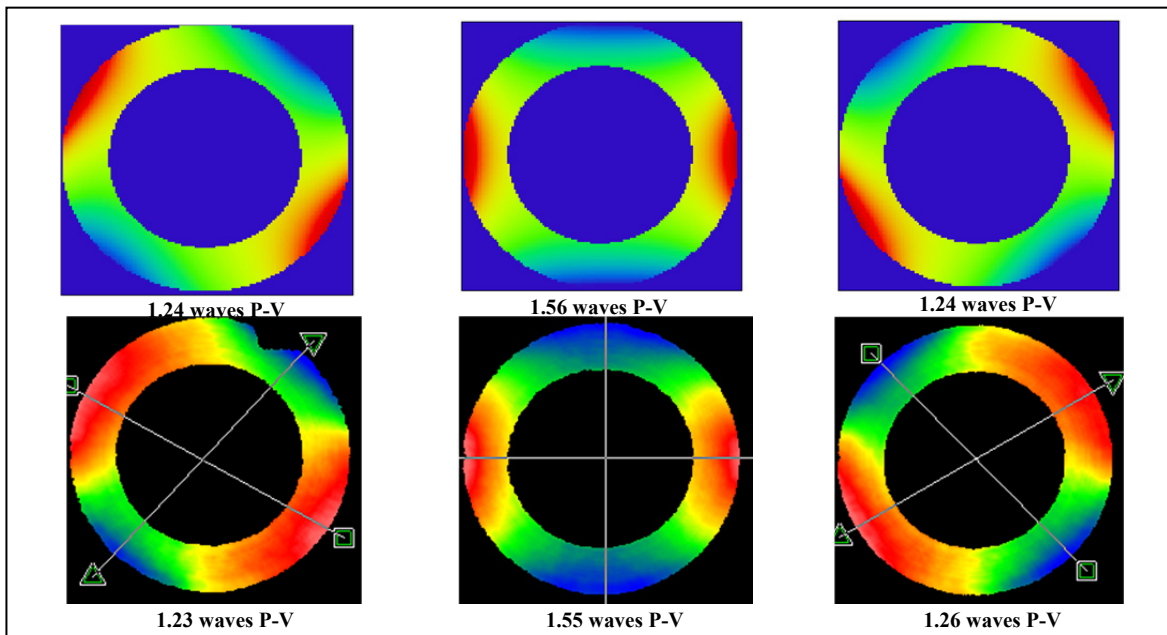


Figure 3: Spectrometer interferograms in 3rd order of (top): nominal design (using Zemax software), and (bottom): aligned NGIS spectrometer. Both sets are at (left to right): top, middle and bottom of the 33.5 degree field. The close match, both of the visual pattern and the P-V wavefront error values, indicates a well-aligned grating.

The warm alignment process locates all the optical elements and the slit but not the focal plane, the grating clocking (rotation of grating lines relative to the slit), or the telescope focus. Once the telescope and spectrometer are individually assembled and aligned, some means is necessary to ensure the initial coarse alignment of these remaining elements. Coarse positioning for the detector and for the grating clocking may simply be based upon mechanical tolerances. The focus position of the telescope with respect to the spectrometer slit may be observed and coarsely adjusted at ambient temperature using another telescope at the front focused at infinity. A visual representation of this process is shown in Fig. 4.

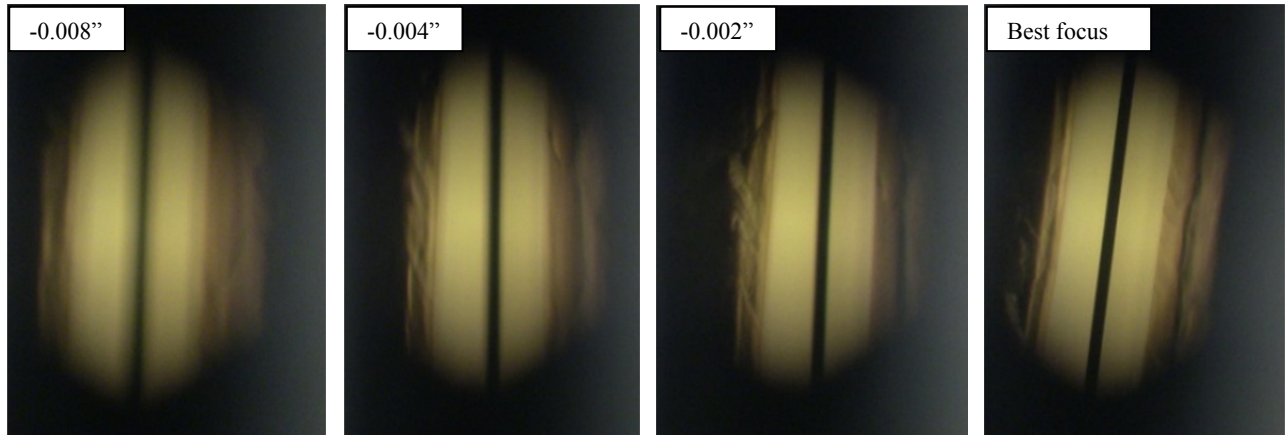


Figure 4: Image of instrument slit as telescope is moved into best focus during warm coarse alignment. (*Left to right*): telescope (moving towards the slit) is out of focus by: $0.008''$, $0.004''$, $0.002''$, and finally at best focus.

3. INSTRUMENT ALIGNMENT AND CHARACTERIZATION TECHNIQUES

Warm alignment of the spectrometer can be invalidated by an inappropriate detector placement, which has the greatest impact on uniformity. This section describes the methods and measurements used for aligning the focal plane and characterizing the instrument. It is important that the diagnostics for alignment bear similarity to the means of final characterization. In our case, we use the same techniques for both.

The three response functions mentioned previously (SRF, CRF, ARF) are used to characterize the spectrometer system. The response functions represent the system response to a delta function input, whether spectral (e.g. a laser) for SRF, or appropriately oriented spatial (small, subpixel slit) for CRF and ARF.

It can be stated to a reasonable approximation that the SRF is a characteristic of the spectrometer portion only, the ARF is a characteristic of the telescope, and the CRF is a characteristic of the complete system. This approximation holds when the spectrometer provides the limiting system aperture, and when the slit is at least as wide as the diffraction spot size (Airy disk) for the longest wavelength.

The effective decoupling of the three response functions permits us to derive independent information about the state of focus of the FPA and telescope separately as well as the clocking errors of detector and grating, and use this information to inform the necessary adjustments. In theory, a single observation or measurement of these functions after warm alignment should suffice to inform all adjustments. In practice, it is found that an iterative process is needed, with the number of iterations depending on the accuracy of the initial warm alignment.

3.1 Measurement techniques

In order to measure the instrument response functions, we have developed a specific stimulus setup called the Penta-Beam Illumination Platform (P-BIP). A rendering of the setup is shown in Fig. 5. The platform employs similar techniques to those used on other imaging spectrometers like AVIRIS⁹, CHRIS¹⁰ and COMPASS¹¹ in that it utilizes an input placed at the focus of an off-axis paraboloid (OAP) collimator mirror as the object generator. The long focal length of the collimator (as compared to the focal length of the NGIS telescope) reduces the placement accuracy at the object space and facilitates the overall construction.

For the spatial (ARF and CRF) measurements, a stimulus slit illuminated by white light is used to simulate a delta function input. The slit measures $130\ \mu\text{m}$ wide in the object space of the collimator and has an image size of $3.3\ \mu\text{m}$ at the system slit location. The stimulus slit is positioned on a motorized stage to move through focus of the OAP. It is turned either parallel or perpendicular to the instrument slit in order to perform the appropriate sub-pixel slit scanning for ARF or CRF measurements, respectively.

Five independent fold mirrors are used to steer the light from the OAP into the entrance pupil of the NGIS instrument. We thus simultaneously achieve illumination from five distinct field angles spanning most of the 33.5° field. It should be noted that if the instrument could easily be rotated continuously, then ARF and CRF measurements would be obtained in a continuous sweep for all locations, instead of just five. Since such a rotation is difficult to impart with the instrument in its vacuum container, this setup is useful for simultaneously recording data at multiple field points without re-adjusting the field angle and repeating the process multiple times.

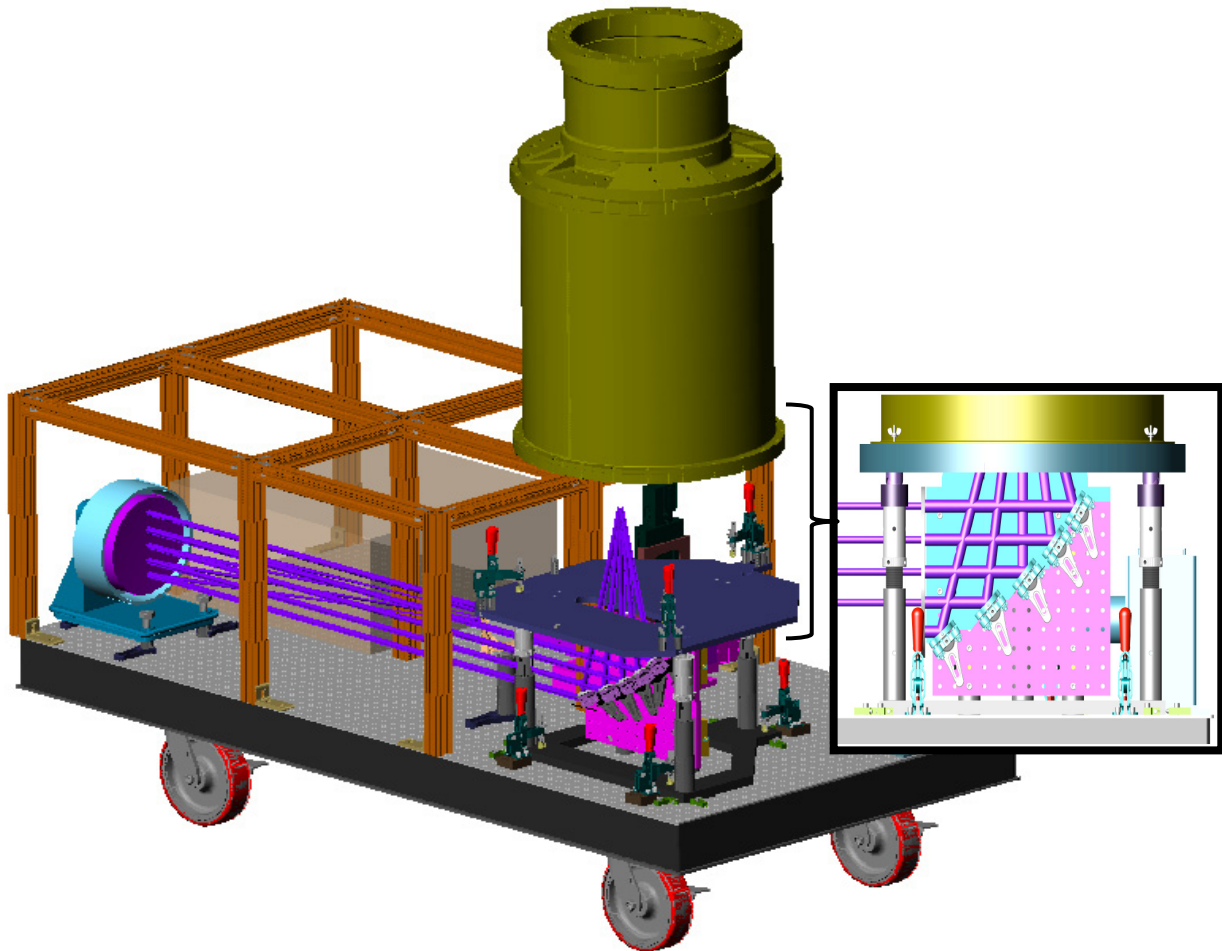


Figure 5: The Penta-Beam Illumination Platform (P-BIP), used for ARF, CRF and SRF measurements. Five independent fold mirrors steer light from the off-axis paraboloid (OAP) collimator and into the instrument entrance pupil. (Left): The instrument is shown suspended above its resting position to reveal the setup. (Right, close-up): Instrument is sitting as expected.

3.2 Along-track response function (ARF) measurements

The ARF measurement is used to inform the focus of the telescope. Results are not affected by spectrometer focal plane misalignments.

In order to measure the ARF, the stimulus slit discussed in section 3.1 is oriented parallel to the instrument slit and scanned in the along-track direction. This measurement is repeated for several focus positions in order to determine the proper focus of the telescope. Using the ratio of the focal lengths of the collimator to the instrument telescope, we may determine the precise adjustment needed to achieve a good ARF. Fig. 6 shows two sets of ARF measurements (both with the test slit at nominal OAP focus), before and after a focus correction.

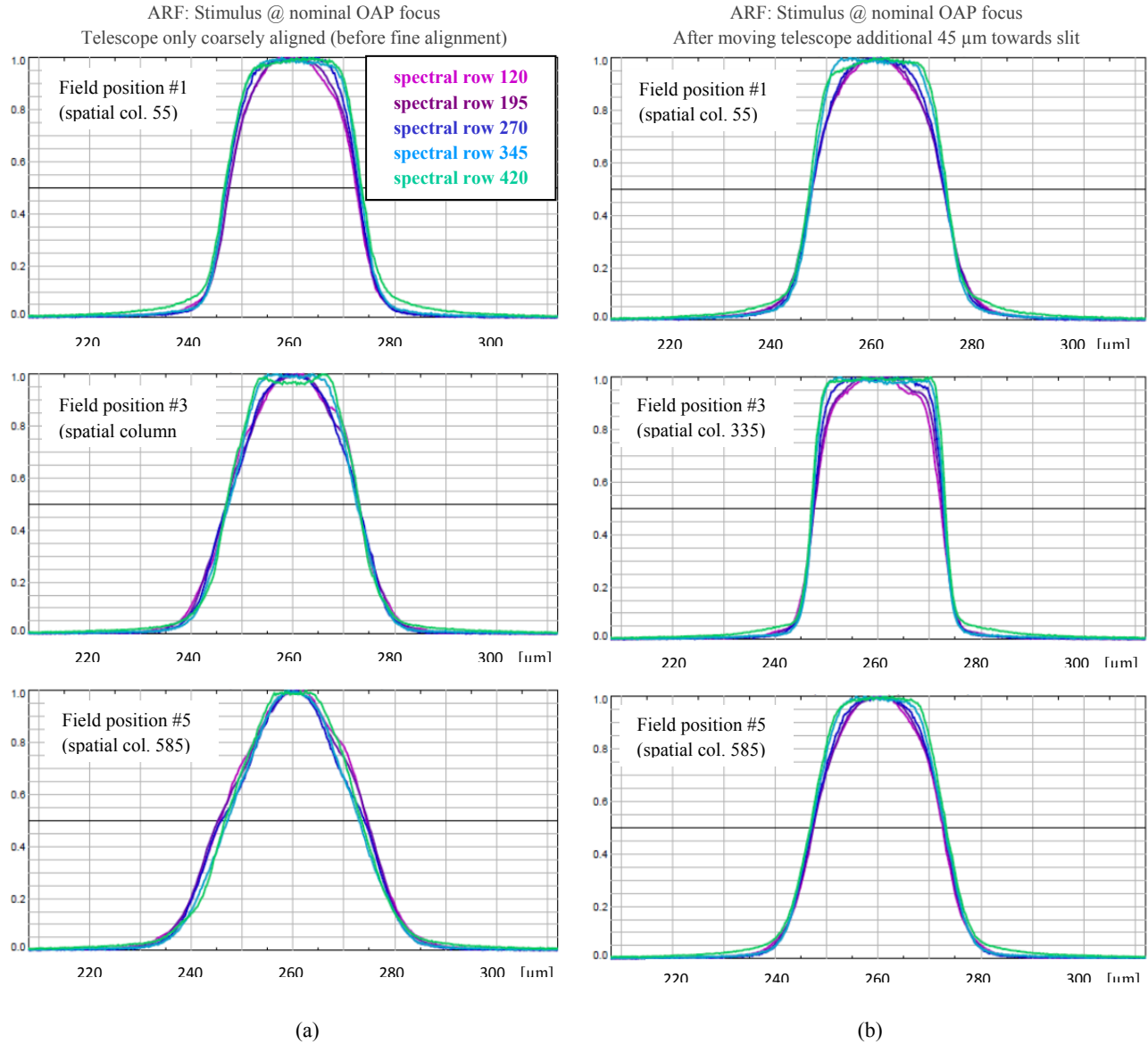


Figure 6: ARF data (with source slit at nominal OAP focus) before (*left, 6a*) and after (*right, 6b*) a telescope focus adjustment of 45 μm . Spatial field positions #1 and #5 are near the edges of the 33.5° instrument field of view. Position #3 is at the middle of the field. The colored curves on each plot represent five spectral channels spanning the wavelength range of the instrument. The horizontal axis is in micrometers of motion at the slit plane.

Between the two sets of measurements in Fig. 6, the telescope was moved 45 μm towards the instrument slit. We see that in the in-focus position (after this adjustment), all ARFs have nearly the same width (uniformity) through wavelength. Although there is some variation across the field, this is not a uniformity requirement, as explained previously.

It should be noted that these measured data essentially represent a static ARF as they do not include motion blur caused by the airborne platform. We take this motion blur into account in Fig. 7 by convolving the measured data (of the focused telescope system from Fig. 6b) with an extra rect function of width equal to one slit (or IFOV). As a result of the extra convolution, the small variation with wavelength observed in Fig. 6 effectively disappears.

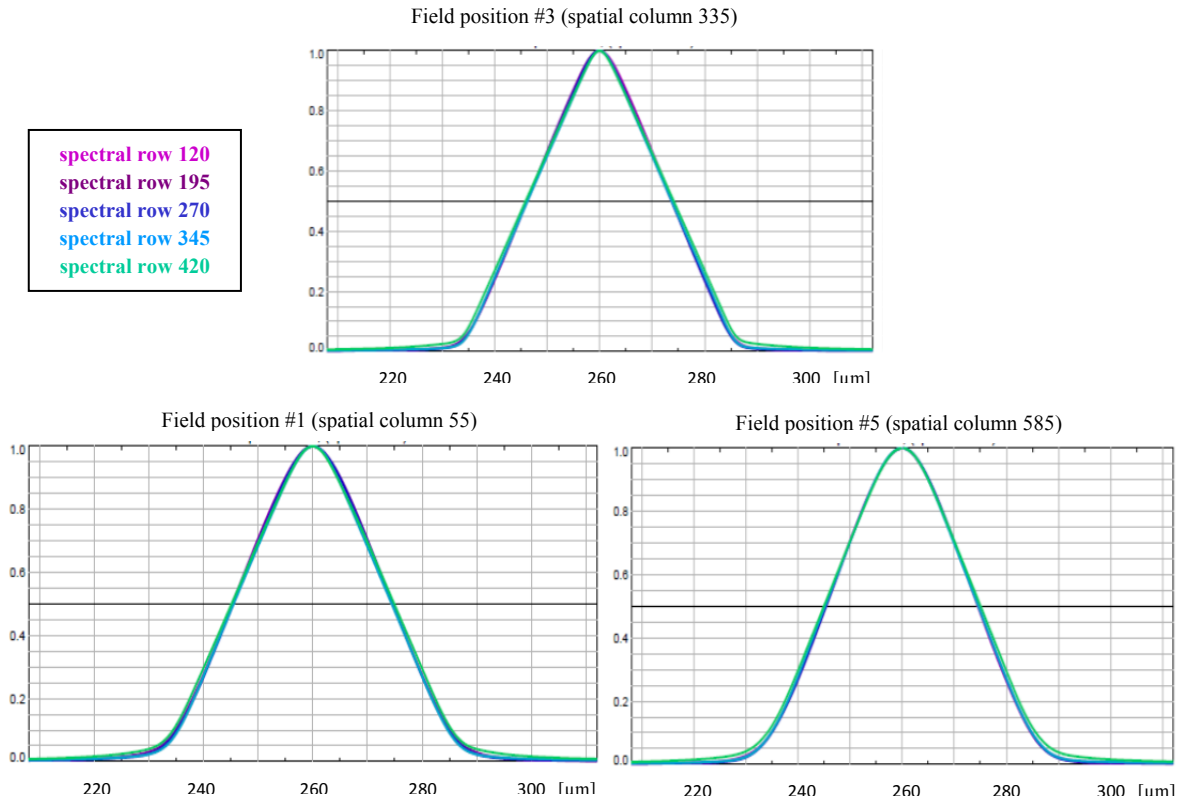


Figure 7: ARF measurements from Figure 6b are convolved with an extra rect function of width equal to that of one slit (or IFOV). This convolution accounts for the motion blur of the airborne platform. Spatial position #3 is at the middle of the field while positions #1 and #5 are near the edges of the 33.5° instrument field of view.

3.3 Cross-track response function (CRF) measurements

The CRF is affected by both the telescope and the spectrometer. However, once the telescope has first been properly focused using ARF data, focal misalignments indicated in the CRF data may be attributed to the detector alone.

The CRF measurement is obtained similarly to the ARF, but with the stimulus slit turned perpendicular to the instrument slit and scanned in the cross-track direction. CRF width is measured across field and wavelength, for various focus positions. This leads to an understanding of the spectral and spatial tilt, as well as the piston (focus) values of the focal plane array position.

Two such through-focus measurements (both at the same detector spatial columns) are shown in Fig. 8, displaying the improvement in full-width at half-maximum (FWHM) that would accompany a better detector focus. With the stimulus at the nominal focus of the OAP, the CRF FWHM ranges from 1.15 to 1.22 of channel spacing, with the variation depending upon wavelength. The second measurement, taken after the stimulus was moved an additional 90mm away from the OAP, shows narrower CRFs, with widths between 1.02 and 1.08 of channel spacing. The focus direction that shows improvement indicates the direction of motion for the focal plane to achieve better focus. The magnitude of such an adjustment would be based upon the 90mm value here and the longitudinal magnification of the collimator/instrument telescope system. In our case, these measurements are indicative of a 60 μm piston correction needed for this particular spatial column.

Given that the CRF functions shown in Fig. 8 do not vary much with wavelength, it may be surmised that the detector does not exhibit significant spectral tilt. In order to observe spatial tilt, these CRF measurements (through focus for spatial columns 320-324 only) would have to be compared to CRFs taken at other parts of the field.

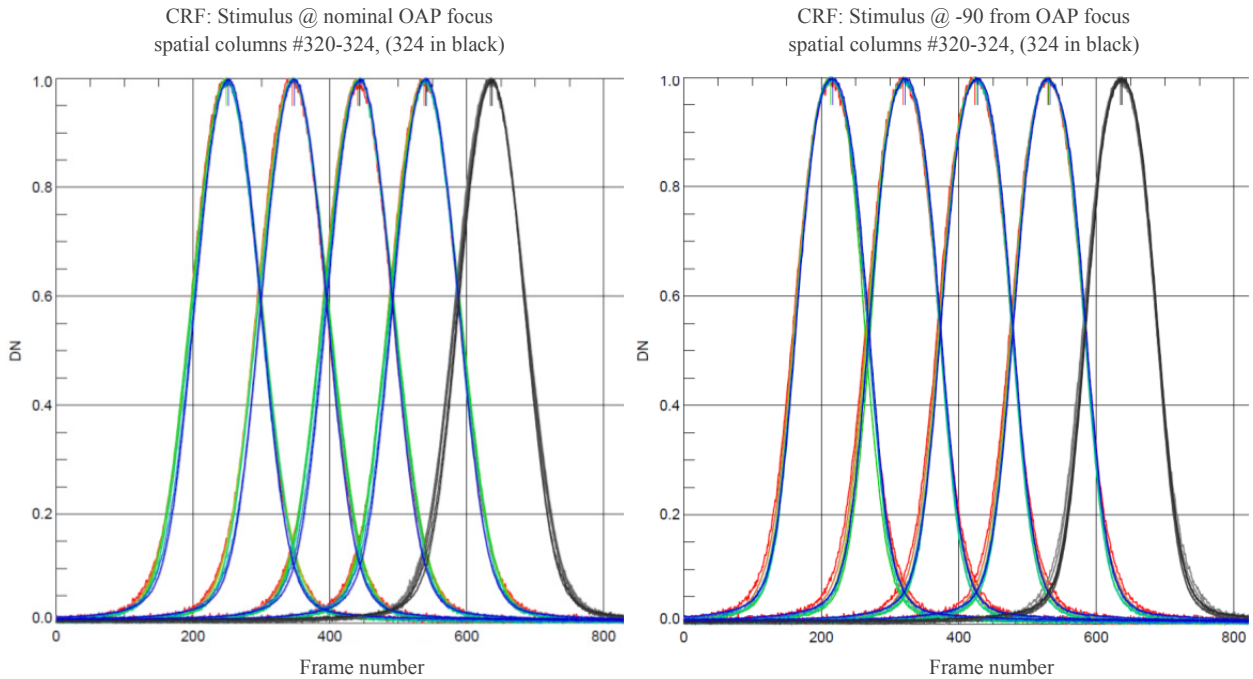


Figure 8: CRF measurements taken at varying stimulus focus. Both display spatial columns 320-324 (of 600 total) and the same wavelengths spanning the spectral range. *Left*: CRF taken at nominal stimulus focus shows FWHM ranging from 1.15 to 1.22 of channel spacing, with the small variation due to wavelength. *Right*: CRF after stimulus has been moved 90mm away from the OAP shows narrower FWHMs of 1.02 to 1.08 of channel spacing.

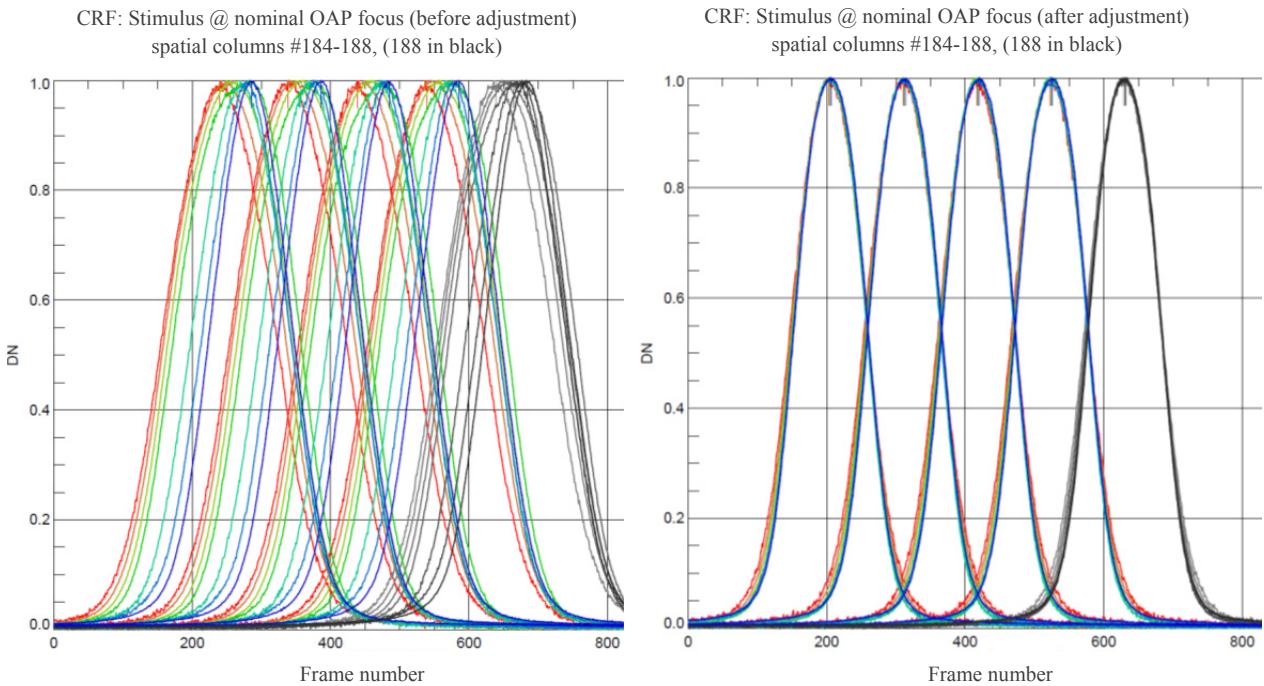


Figure 9: CRF measurements before and after FPA focus adjustment. Both are for the same spatial columns (184-188 of 600 total), and both contain several sample wavelengths spanning the full spectral range. *Left*: FWHM spans 1.3 to 1.9 of a pixel, depending upon wavelength. *Right*: After a detector piston adjustment of 85 μm (at these spatial columns), FWHM measures 1.06 to 1.10 of a pixel. Additionally, a 1.0 mrad grating clocking adjustment leads to more uniform centroid locations through wavelength.

In addition to using CRF width for spectrometer focus, we use the CRF peak/centroid location as a function of wavelength to indicate the grating clocking. It should be noted that if the focal plane is clocked relative to the slit, this will affect the apparent grating clocking observed in the CRF. The focal plane clocking error should thus be added to or subtracted from the apparent grating clocking to determine the actual grating clocking error needing correction.

Sample CRF measurements taken before and after an adjustment involving both detector piston and grating clocking are given in Fig. 9. Both measurements are for detector columns 184 to 188 (of 600 total), and both contain several sample wavelengths spanning the full wavelength range. The adjustment made between the two measurements involved a piston of 85 microns at this area of the detector, and a grating clocking of 1.0 mrad (after accounting for the detector clocking). This resulted in a) this part of the detector moving into better focus (as indicated by the widths narrowing from ~ 1.6 to < 1.1 of pixel spacing), and b) an improved grating clocking (indicated by the coincident CRF centroid locations through wavelength).

3.4 Spectral response function (SRF) measurements

The spectral characteristics of a spectrometer and its accurate spectral calibration are the most critical pieces of knowledge required for reliable spectroscopy. This information comes from the SRF, which we obtain through two types of measurements: 1) Width measurements, made using a scanning monochromator on the P-BIP platform, and 2) Centroid location uniformity measurements using a whole-field laser illumination method.

The whole-field laser illumination, or “laser sphere,” measurement is performed with the instrument suspended in a gantry such that the entrance pupil may be illuminated with a series of lasers fed through an integrating sphere. This technique provides a simple means of measuring centroid uniformity, but does not provide reliable SRF width data as the function is too sparsely sampled. Also, there are only a few laser wavelengths, so only a limited set of SRF widths could be produced. The centroid location uniformity data is useful in visualizing and correcting for detector clocking. Fig. 10 shows laser sphere centroid data at a given wavelength (407 nm) before and after a detector clocking adjustment of 4% of a pixel. While not shown in the figure, it should be noted that laser lines at other wavelengths indicate the same clocking. When fully clocked as shown, the overall smile (as residual slit image curvature) measured with this instrument at the worst-case wavelength was 3% of a pixel ($\sim 0.8 \mu\text{m}$).

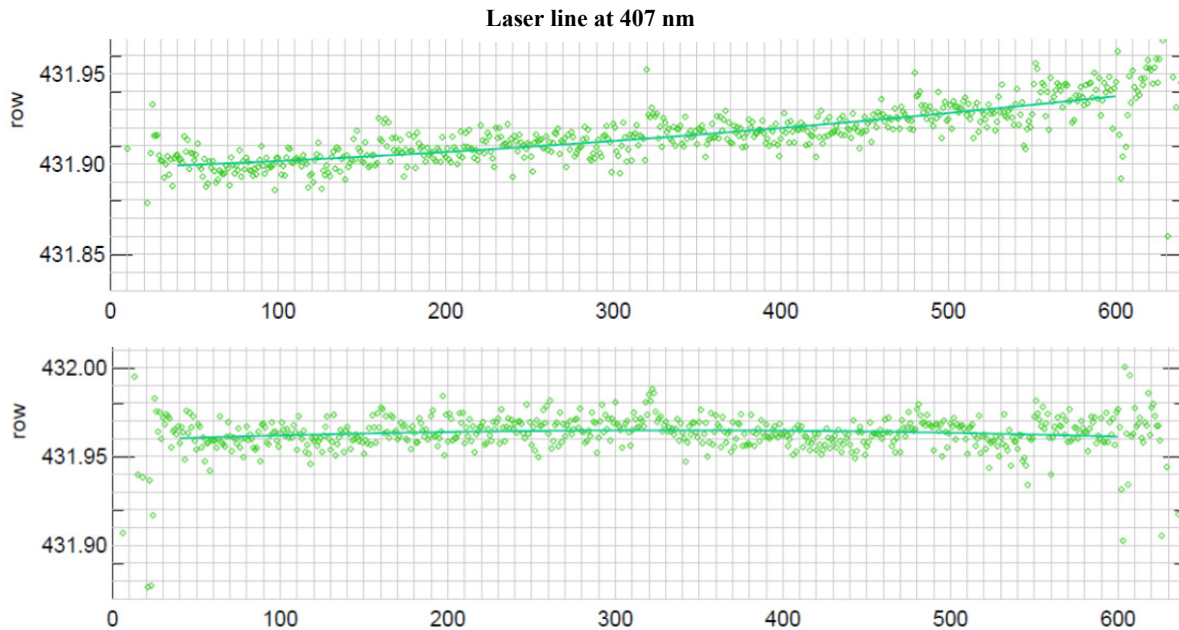


Figure 10: Whole-field laser illumination measurements at the 407 nm laser line. *Top*: Centroids indicate a clocking error of 4% of a pixel across the detector. *Bottom*: Post-detector clocking adjustment. Horizontal axis is in spatial columns of the detector (640 total columns).

The SRF width measurements, spanning the full 380-2510 nm spectral range are made using a scanning monochromator. Sample measurements are given in Fig. 11 for two spectral regions. The frame numbers along the horizontal axis may be matched to specific wavelengths based on a spectral calibration, and there is 5nm spacing between peaks. Five spatial columns spanning the field of the instrument are overlaid for comparison. The data shows maximum spatial variation of 4% in the 1230 nm spectral region and a maximum spatial variation closer to 10% in the 2220 nm spectral region.

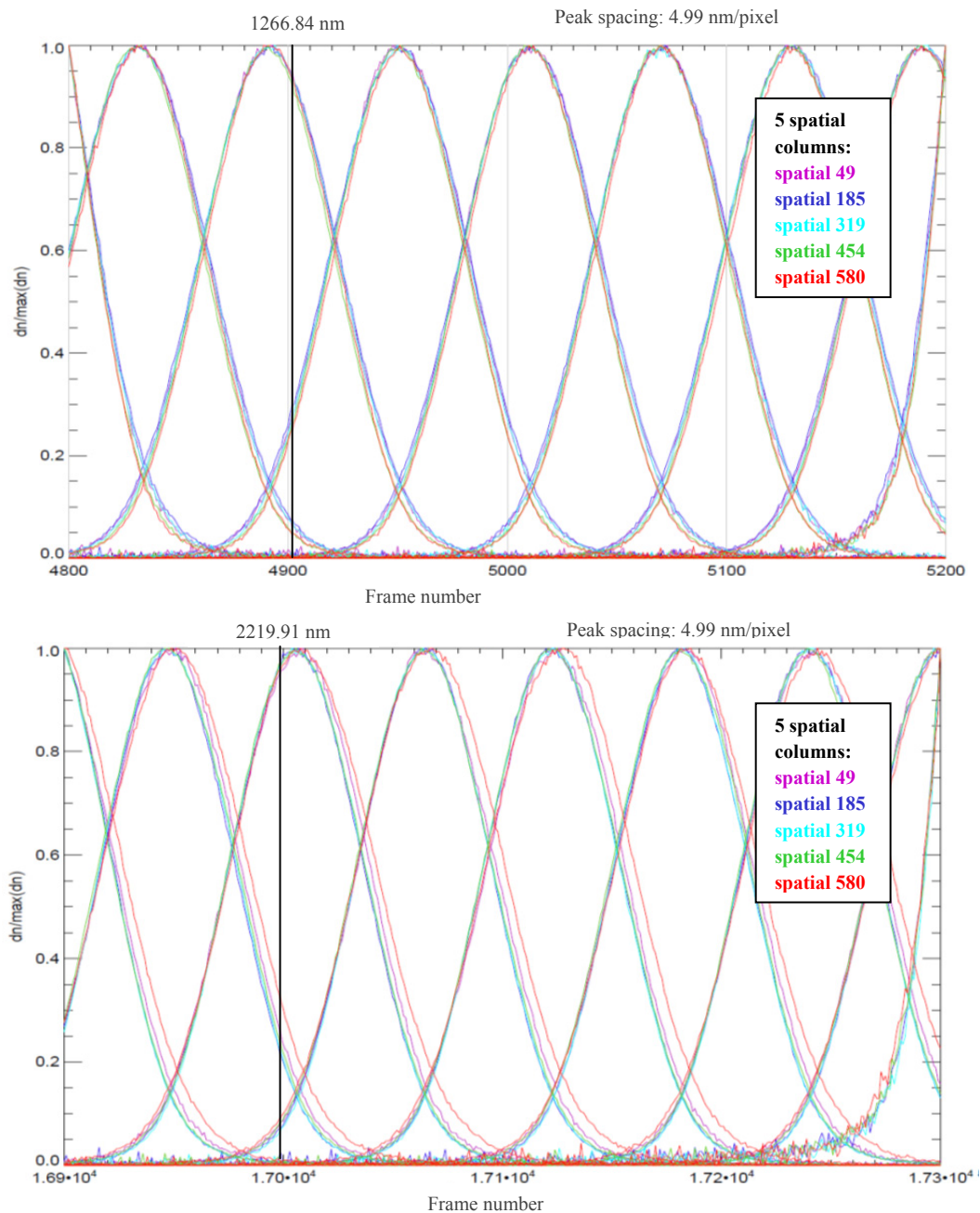


Figure 11: SRF measurements at two sample spectral regions. Spacing between peaks is 5 nm. *Top*: In the spectral region of 1265 nm, maximum spatial variation is 4%; *Bottom*: At 2220nm, maximum spatial variation is 10%. The colored curves on each plot represent five spatial channels spanning the field.

Note that the SRF is inherently broader than the ARF or CRF. While the latter two functions can be thought of as convolutions of either the slit or the pixel response with the line spread function, there are four factors contributing to the width of the SRF: the slit, the pixel response, the line spread function, and the grating resolving power. The width of the measured SRF is also affected by the monochromator response (FWHM of 2 nm). This factor is not deconvolved from the data shown in Fig. 11.

Although we typically use the CRF data in adjusting the detector focus, it is expected that the SRF will improve simultaneously. For example, as a result of the detector piston and tilt adjustment shown with CRFs in Fig. 9, we also observed an improvement in the SRF width by 13% and 26% at the two ends of the spectrum.

4. CONCLUSIONS

Using measured data from the NGIS instruments, we have demonstrated key methods for aligning and characterizing imaging spectrometers to achieve high levels of uniformity. Smile, keystone, grating rotation, and detector rotation errors have been kept below 5% of a pixel and typically under 3%. Response function non-uniformity was kept to less than 10% of FWHM variation through field or wavelength. In order to build an instrument capable of achieving these results, correspondingly sensitive alignment processes and techniques must be devised, using the same methods of characterization as during instrument calibration. Preliminary alignment processes at ambient temperature were discussed, which, with an athermalized opto-mechanical design, permit us to concentrate only on relatively few parameters requiring adjustment derived from information at operating temperature (cold cycles). Those parameters are the precise detector location and orientation, the grating clocking, and the telescope precise focus. The type of measurement that informs each of these parameters and the improvements upon subsequent adjustment were also shown.

ACKNOWLEDGMENTS

The research in this paper was performed at the Jet Propulsion Laboratory, California Institute of Technology under contract with the National Aeronautics and Space Administration. We thank the Next-Generation Imaging Spectrometer (NGIS) team for their support. Reference herein to any specific commercial product, process or service by trade name, trademark, manufacturer, or otherwise, does not constitute or imply its endorsement by the United States Government or the Jet Propulsion Laboratory, California Institute of Technology.

REFERENCES

- [1] P. Mouroulis, R.O. Green, and T.G. Chrien, "Design of pushbroom imaging spectrometers for optimum recovery of spectroscopic and spatial information," *Appl. Opt.* 39, 2210-2220 (2000).
- [2] R.O. Green, "Spectral calibration requirement for Earth-looking imaging spectrometers in the solar-reflected spectrum," *Appl. Opt.* 37, 683-690 (1998).
- [3] R.A. Neville, L. Sun, and K. Staenz, "Detection of spectral line curvature in imaging spectrometer data," *Algorithms and Technologies for Multispectral, Hyperspectral and Ultraspectral Imagery IX*, Proc. SPIE, 5093, 144-154 (2003).
- [4] R.A. Neville, L. Sun, and K. Staenz, "Detection of keystone in imaging spectrometer data," *Algorithms and Technologies for Multispectral, Hyperspectral, and Ultraspectral Imagery X*, Proc. SPIE, 5425, 208-217 (2004).
- [5] H.A. Bender, P. Mouroulis, R.O. Green, D.W. Wilson, "Optical design, performance and tolerancing of next-generation airborne imaging spectrometers," *Imaging Spectrometry XV*, Proc. SPIE, 7812, 78120P-1-78120P-12 (2010).
- [6] A. Offner, "Unit power imaging catoptric anastigmat," U.S. Patent No. 3,748,015 (1973).
- [7] L. Mertz, "Concentric spectrographs," *Appl. Opt.*, 16, 3122-3124 (1977).
- [8] P. Mouroulis, and M. McKerns, "Pushbroom imaging spectrometer with high spectroscopic data fidelity: experimental demonstration," *Opt. Eng.* 39, 808-816 (2000).
- [9] T. Chrien, R.O. Green, C.J. Chovit, M.L. Eastwood, and C.M. Sarture, "Calibration of the Airborne Visible/Infrared Imaging Spectrometer in the Laboratory," JPL Publication 99-1, JPL, Pasadena, CA (1999).
- [10] M.A. Cutter, D.R. Lobb, T.L. Williams, and R.E. Renton, "Integration & Testing of the Compact High-Resolution Imaging Spectrometer (CHRIS)," *Imaging Spectrometry V*, Proc. SPIE 3753, 180-191 (1999).
- [11] J. Zadnik, D. Guerin, R. Moss, A. Orbeta, R. Dixon, C. Simi, S. Dunbar, and A. Hill, "Calibration Procedures and Measurements for the COMPASS Hyperspectral Imager," *Algorithms and Technologies for Multispectral, Hyperspectral, and Ultraspectral Imagery X*, Proc. SPIE, 5425, 182-188 (2004).